Design, characterization and modelling of the Charge eXchange Recombination Spectroscopy (CXRS) suite at the SMall Aspect Ratio Tokamak (SMART)

D. J. Cruz-Zabala,[1] E. Viezzer,[1] A. Rodriguez-Gonzalez,[1] J. Segado-Fernandez,[1] A. Alvarado-Reyes,[1] J. Perez-Gonzalez,[1] M. Garcia-Munoz,[1] and R. Dux[2]
[1)]*Department of Atomic, Molecular and Nuclear Physics, University of Seville, Seville, 41012, Spain*
[2)]*Max-Planck-Institut für Plasmaphysik, Garching, 85748, Germany*

(Dated: 1 July 2024)

Ion temperature, rotation, and density are key parameters to evaluate the performance of present and future fusion reactors. These parameters are critical for understanding ion heat, momentum, and particle transport, making it mandatory to properly diagnose them. A common technique to measure these properties is Charge eXchange Recombination Spectroscopy (CXRS). For characterizing positive and negative triangularity plasmas at the SMall Aspect Ratio Tokamak (SMART), a poloidal array of gas puff based CXRS diagnostics will be measuring the ion properties in different poloidal positions. In this work, the modelling of the expected signal and spatial coverage using the FIDASIM code is presented. Furthermore, the design and characterization of the Low Field Side (LFS) midplane CXRS diagnostic are described. Each diagnostic is composed of a gas injection system, an optical system that collects the light emitted by the plasma, and a spectrometer. These systems will provide ion temperature, rotation, and density with a radial resolution of 3.75 mm and a temporal resolution of 2.2 ms.

I. INTRODUCTION

The triple product of density, temperature, and energy confinement time is an indication of the fusion performance of a confined plasma, making it indispensable to properly characterize these parameters. There are several ways to measure the electron temperature and density. However, there are fewer techniques to measure the ion properties. One of the most common techniques for measuring ion properties is Charge eXchange Recombination Spectroscopy (CXRS)[1]. This technique extracts the ion temperature, rotation, and density from the light emitted after the charge transfer between injected neutrals and ionized ions from the plasma. Therefore, CXRS requires a source of neutrals to induce light emission. Charge eXchange (CX) reactions commonly occur due to background neutrals coming from the Scrape of Layer (SOL) region. However, the light emission due to these reactions is not well localized and it is complicated to assign a spatial location to it. The CXRS technique needs a localized source of neutrals that will allow us to determine the location of the emission and, hence, of the measurement. Three options are normally used: a neutral beam injection system (NBI), a diagnostic neutral beam (DNB), or a gas puff (GP). NBI systems are used to heat the plasma, but CXRS diagnostics can take advantage of the high energy neutrals injected by such a system to produce the CX reactions. DNB systems are similar to NBI systems, but operate at lower power, reducing their impact on the plasma. GP systems inject low energetic neutrals that penetrate less into the plasma compared to NBI and DNB. CXRS diagnostics based on GP (GP-CXRS) have some interesting advantages[2]. First, it is easier to install them around the vessel wall due to their reduced size. Second, they are much cheaper than NBI and DNB. Third, the measurements provided at the edge are more accurate because of the higher neutral density produced by GP-CXRS in this region and the more localized emission. The main drawbacks of GP-CXRS are the limited penetration of the injected neutrals and the large molecular emission if molecules are injected. However, these molecular emissions can be removed by advanced fitting processes[3].

In the confined region of tokamak plasmas, main ion and electron pressures are expected to be, to a large degree, constant on a flux surface[4]. However, poloidal asymmetries in the impurity rotation and density have been found at the plasma edge in different tokamaks, such as ASDEX Upgrade[3,5,6] and Alcator C-Mod[7,8]. In order to characterize these poloidal asymmetries, CXRS diagnostics measuring in different poloidal locations are needed. Efforts have been made in ASDEX Upgrade[9] and Alcator C-Mod[2] to install CXRS diagnostics at the HFS region. However, diagnostics in more poloidal positions are desirable to obtain a complete picture of the ion properties along a complete flux surface[10]. All previous studies on the poloidal dependence of the ion properties were performed in positive triangularity (PT) plasmas, which means a plasma geometry similar to a "D". However, it would be interesting to study this for negative triangularity (NT) plasmas as well. NT plasmas are characterized by an inverse "D" geometry and show important advantages compared to PT plasmas. These plasmas show high performance with the absence of Edge Localized Modes (ELMs)[11,12], which are cyclic instabilities that expel particles towards the wall that can damage the reactor. Furthermore, Low Field Side (LFS) profiles in NT show differences when compared to PT plasmas as there is no pedestal in the edge region. These special characteristics of NT plasmas and the poloidal dependence of the ion properties observed in PT plasmas motivate the development of a poloidal array of CXRS systems for the SMall Aspect Ratio Tokamak (SMART).

SMART[13–15] is a spherical tokamak (ST) that is being commissioned at the University of Seville that aims to compare the performance of PT and NT plasmas at low aspect ratio (ratio

between major and minor radius). STs[16–18] show high performance and are more compact than conventional tokamaks, which might reduce the cost of a possible future fusion power plant based on this concept. The combination of ST operating in NT might be a game changer for future fusion power plants and SMART aims to address it.

This paper is structured as follows: section II discusses the modelling performed using the FIDASIM code to estimate the expected signal of these diagnostics. Section III shows the design and characterization of the first diagnostic of the full poloidal array of GP-CXRS systems at SMART. A summary and an outlook are given in section IV.

II. SYNTHETIC SIGNAL CALCULATION USING FIDASIM

To provide measurements at different points along the poloidal direction, six GP-CXRS diagnostics have been planned for the SMART tokamak. These six systems will be split between LFS and HFS. The first step in the design of such a suite of diagnostics is a feasibility study. In this work, the GP module[3] of the FIDASIM code[19,20] has been used to calculate the neutral density produced by these GP systems. FIDASIM launches Monte Carlo (MC) markers following an initial distribution that simulates the observed gas cloud shape in laboratory experiments at ASDEX Upgrade[9]. These MC markers travel around the edge of the plasma and can produce CX reactions with the main ions of the plasma, producing another generation of neutrals. Note that in the cases considered here, the species of the injected neutrals coincide with the main ion species. These new neutrals can suffer again CX with other main ions, producing successive generations of neutrals. These are the so-called halo neutrals. Figure 1 shows the first generation of neutrals produced by the GP-CXRS suite at SMART simulated with FIDASIM. Note that this generation of neutrals does not penetrate much due to its low energy. Halo neutrals penetrate deeper into the plasma and are the main responsible for CX emission in the confined region[3].

The measured radiance depends on the neutral density but also on the density of the measured species. Specifically, the expected radiance can be calculated as follows:

$$L_{CX,\alpha,\lambda} = \frac{h\nu}{4\pi} \sum_n \int_{LOS} n_{D,n}(s) n_\alpha(s) \langle \sigma_{n,\alpha,\lambda} v_j \rangle_{eff}(s) ds \quad (1)$$

where $h\nu$ is the energy of the photons, $n_{D,n}(s)$ is the total neutral density of the main ion species (hydrogen in this case) at each point s along the line of sight (LOS), $n_\alpha(s)$ is the density of the measured species, $\langle \sigma_{n,\alpha,\lambda} v_j \rangle_{eff}(s)$ is the CX emission rate, and the sub-index n represents the principal quantum number. In SMART, carbon is expected to be the main impurity in plasma. Considering a case where a flow rate of $5 \cdot 10^{20}$ part/s, which is similar to the values used at ASDEX Upgrade, is injected at the LFS midplane and a value of the effective charge of $Z_{eff} = 3.0$, the previous equation can be solved providing the carbon radiance profile shown in figure 2. This radiance corresponds to the $C^{6+}(n = 8 \rightarrow 7)$ line at

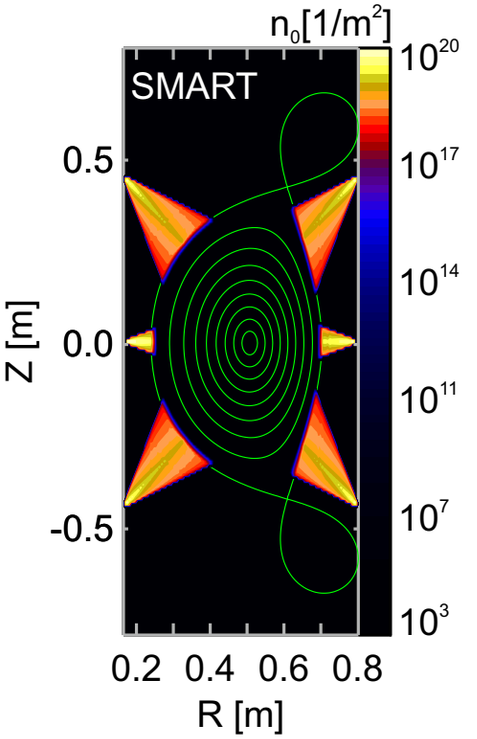

FIG. 1. Density of the first generation of neutrals produced by the poloidal array of GP-CXRS calculated with FIDASIM.

529.059 nm. The horizontal line at 10^{16} ph/(sr·m^2·s) represents an empirical signal threshold obtained from experience at ASDEX Upgrade. It can be seen that the signal stays above this threshold in the range $0.6 \lesssim \rho_{pol} \lesssim 1.0$, which means that measurements of carbon temperature, rotation, and density would be possible in this region. If $Z_{eff} = 2.0$ is considered, this radial range is reduced to $0.7 \lesssim \rho_{pol} \lesssim 1.0$. Other species such as hydrogen (main ion), helium, and nitrogen together with other carbon lines will be explored.

III. DESIGN AND CHARACTERIZATION OF THE LFS MIDPLANE CXRS DIAGNOSTIC

The installation of the GP-CXRS suite at SMART will be done in several steps. The first diagnostic that will be installed is the one at the LFS midplane. This diagnostic will confirm the calculations shown in the previous section and will allow us to identify challenges and possible improvements.

A sketch of the gas injection system is shown in figure 3, which is a simplification of the system shown in[21] and also used in[9]. Two bottles with different gases will be available to supply the system. The pressure reducers PR1 and PR2 together with the valves V1 and V2 will allow us to safely open the gas bottles. A commercial pressure controller PC (model MKS GPCA) will be in charge of setting the requested pressure in the system. This pressure is measured with the pressure sensor PS. A reservoir RE is filled with gas which will

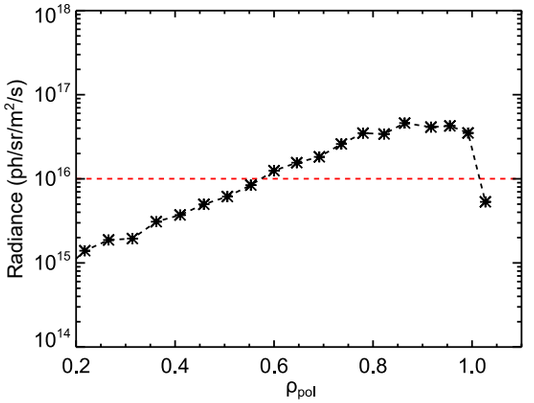

FIG. 2. Radiance of the $C^{6+}(n = 8 \rightarrow 7)$ line expected for the LFS midplane GP-CXRS system. The symbols correspond to the radiance at the measurement positions of the LOS. The red dashed line represents the minimum empirical radiance level required to extract temperature, rotation and density measurements.

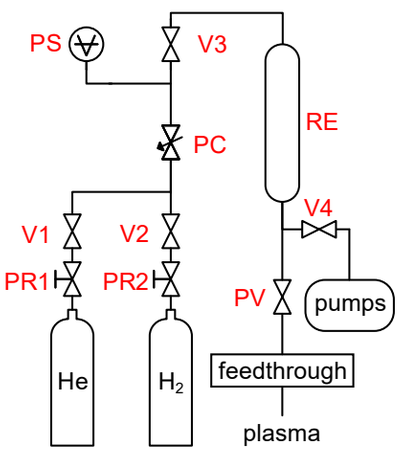

FIG. 3. Sketch of the gas control system of the GP-CXRS diagnostics. He and H_2 bottles are shown, but other gases could also be used.

ensure a constant pressure during a plasma discharge due to its large volume (1 L approx.). Note that the valve V3 is closed during operation. Finally, a fast piezoelectric valve PV (model Key PEV-1) controls the gas injection to the plasma with a response time of 2 ms. This valve enables fast switching of the valve, allowing us to remove the background emission from the active source of light. The valve V4 is activated when pumping is needed.

As commented in the previous section, the gas flows towards the plasma and light is emitted due to CX reactions. The first GP-CXRS system at SMART collects the light emitted at the LFS midplane using 25 toroidally oriented lines of sight (LOS). Figure 4 shows a sketch of a top view of the system. Note that only 5 LOS are shown for clarity, and the GP is shown as a green cone. Figure 4 also shows how the optical components are attached to the vacuum chamber of SMART. The main limitation in terms of radial resolution is given by the LOS spot size at the measurement position, which is $\approx$

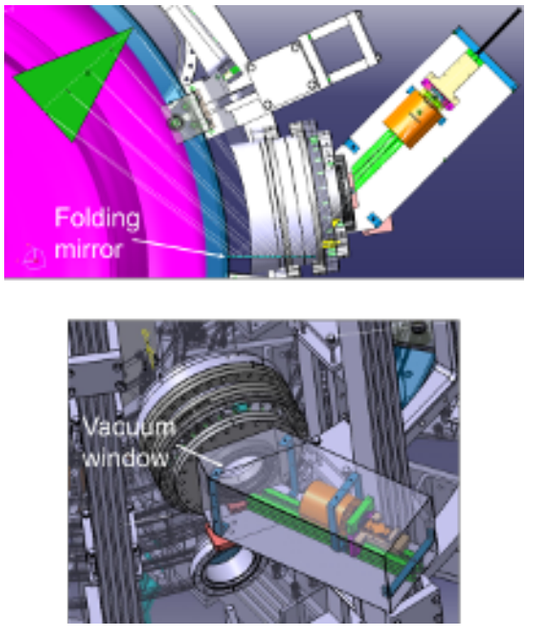

FIG. 4. Top and external view of the optical components of the LFS midplane GP-CXRS system. Five evenly spaced LOS are shown in the top view together with a green triangle simulating the gas cloud shape.

3.75 mm. These 25 LOS are evenly spaced, covering 0.235 m of the plasma radius at the midplane. By default, the covered radial range goes from R = 0.515 - 0.750 m, but small variations are allowed by adjusting the folding mirror. This folding mirror deflects the emitted light towards a vacuum window. A detailed sketch of the out-vessel optical components is shown in figure 5. After exiting the vacuum window, the light is focused by a commercial camera objective (model Canon RF 85mm F2 MACRO IS STM) with a focal length of 85 mm. After the camera objective, another lens is placed to correct for telecentricity. This telecentric lens is tilted 0.64° and decentered with respect to the optical axis by 1.25 mm to optimize the correction. This lens ensures sharp images of the gas cloud emission for all LOS. After the telecentric lens, the 400 µm diameter optical fibers are held by a slit. The optical fibers then travel towards an intermediate connection panel. This panel is also connected to the spectrometer by another fiber bundle. This intermediate panel allows us to modify the connection between the fibers that go to the tokamak vessel and to the spectrometer.

The light transmitted by the fibers finally enters a Czerny-Turner spectrometer. The light is collimated after passing through the entrance slit (60 µm) and then dispersed by a 2400 grooves/mm grating and focused onto a charge-coupled device (CCD) camera (model Teledyne Princeton Instruments ProEM-HS:1024XB). This camera has 1024×1024 13 µm width pixels. The central wavelength on the chip can be changed by moving the grating through a motor. This enables measurements of different impurities such as nitrogen (566.937 nm, $n = 9 \rightarrow 8$), boron (494.467 nm, $n = 7 \rightarrow 6$), he-

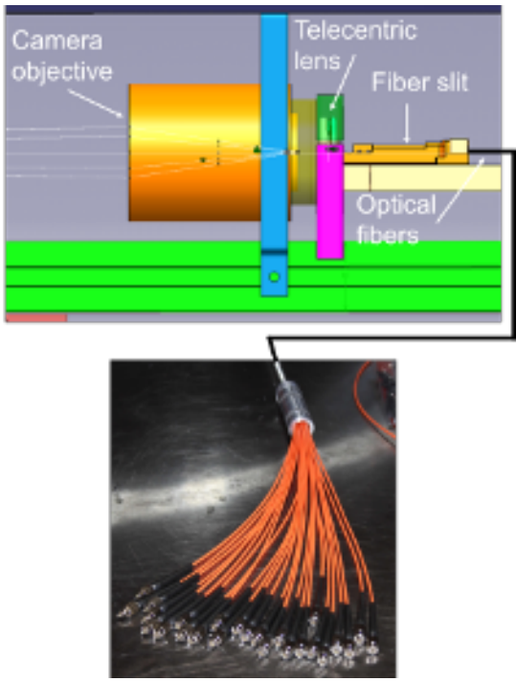

FIG. 5. Sketch showing the details of the optical components of the LFS midplane GP-CXRS system. A picture of the fiber bundle is also shown. These fibers are connected to another fiber bundle that brings the light to the spectrometer.

lium (468.571 nm, $n = 4 \rightarrow 3$) or neon (524.897 nm, $n = 11 \rightarrow 10$). The lenses used in this spectrometer are made of fused silica, which produces high chromatic aberration. The chromatic aberration is a type of optical distortion that is produced by the dependence of the refractive index on the wavelength of the light. To counteract this effect, three additional motors are installed: one in the entrance objective, one in the camera objective and another one in the camera itself. These additional motors allow us to focus a specific wavelength onto the camera. The spectrometer can handle up to 25 fibers that can be imaged on the camera simultaneously every 2.2 ms. The channels are distributed along the y axis of the camera chip while the x axis corresponds to the wavelength. At a central wavelength of 567 nm, the covered spectral range is ≈ 15 nm with a dispersion $d\lambda/dpix$ of 0.017 nm/pix. Figure 6 shows a picture of the described spectrometer. Once the spectra have been recorded, fitting techniques together with background subtraction are performed to obtain the temperature and rotation of the measured species. A shot-to-shot wavelength calibration is performed to improve the rotation measurements. For the evaluation of the density, the measured radiance together with the modelled neutral density (as shown in section II) are required. An integrating sphere (model Gigahertz-Optik ISS-17-VA-V01) is used to perform the absolute intensity calibration of the full system.

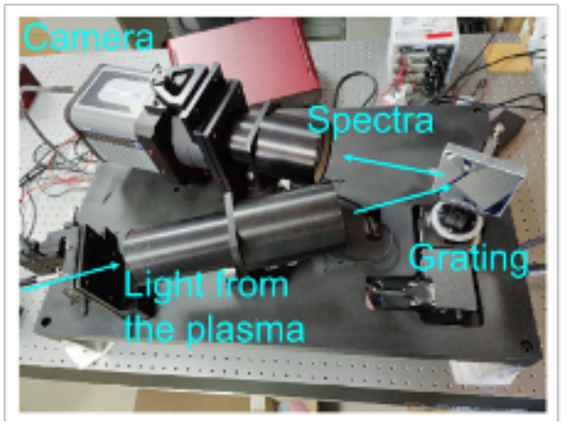

FIG. 6. Picture of the spectrometer that will be used in the LFS midplane GP-CXRS system. In real operation, the spectrometer will be covered so that external light does not enter in the system.

IV. SUMMARY AND OUTLOOK

The poloidal array of GP-CXRS of the SMART tokamak is introduced. These diagnostics will provide radial profiles of the temperature, rotation, and density of the measured ion species in different poloidal locations. In order to estimate the expected signal of these diagnostics, the neutral density produced by the GP was simulated using the FIDASIM code. For the $C^{6+}(n = 8 \rightarrow 7)$ emission line, the expected radiance is high enough to extract measurements from approximately mid-radius to the separatrix. This range might change depending on the measured species. This will also change depending on the Z_{eff} and the plasma density and temperature profiles. The design of the first GP-CXRS diagnostic, which will be measuring at the LFS midplane, is described. It is composed by a gas injection system, the optical system, and a spectrometer. The gas injection allows us to separate between active light and background light by means of a fast piezoelectric valve. The optical system is composed by a folding mirror, a camera objective, a telecentric lens, and a fiber bundle. It transmits the light from the tokamak vessel towards the spectrometer. The radial resolution is given by the LOS spot size at the measurement position, which is ≈ 3.75 mm. Finally, the light is analyzed by means of a spectrometer. This spectrometer can handle up to 25 fibers with a time resolution of 2.2 ms and a wavelength resolution of 0.017 nm/pix. Four motors allow us to change and focus the central wavelength of the spectrometer. After subtracting the background emission, the measured spectra are fitted, and the temperature and rotation of the measured species are extracted. Density can be extracted from the measured radiance and the modelled neutral density.

ACKNOWLEDGMENTS

The first author gratefully acknowledges the funding from the EUROfusion consortium under the "Bernard Bigot" Re-

searcher Grant programme (grant agreement AWP23-ERG-CIEMAT/Cruz Zabala).

This work has been carried out within the framework of the EUROfusion Consortium, funded by the European Union via the Euratom Research and Training Programme (Grant Agreement No 101052200 — EUROfusion). Views and opinions expressed are however those of the author(s) only and do not necessarily reflect those of the European Union or the European Commission. Neither the European Union nor the European Commission can be held responsible for them.

DATA AVAILABILITY

The data that support the findings of this study are available from the corresponding author upon reasonable request.

REFERENCES

[1]R. J. Fonck, D. S. Darrow, and K. P. Jaehnig, "Determination of plasma-ion velocity distribution via charge-exchange recombination spectroscopy," Physical Review A **29** (1984).

[2]R. M. Churchill, C. Theiler, B. Lipschultz, R. Dux, T. Pütterich, and E. Viezzer, "Development of the gas puff charge exchange recombination spectroscopy (gp-cxrs) technique for ion measurements in the plasma edge," Review of Scientific Instruments **84** (2013), 10.1063/1.4821084.

[3]D. J. Cruz-Zabala, E. Viezzer, U. Plank, R. M. McDermott, M. Cavedon, E. Fable, R. Dux, P. Cano-Megias, T. Pütterich, A. J. van Vuuren, M. Garcia-Munoz, J. G. Lopez, and T. AUG, "In-out charge exchange measurements and 3d modelling of diagnostic thermal neutrals to study edge poloidal impurity asymmetries," Plasma Physics and Controlled Fusion (2022), 10.1088/1361-6587/AC5917.

[4]F. L. Hinton and R. D. Hazeltine, "Theory of plasma transport in toroidal confinement systems," Reviews of Modern Physics **48**, 239 (1976).

[5]T. Pütterich, E. Viezzer, R. Dux, and R. M. McDermott, "Poloidal asymmetry of parallel rotation measured in asdex upgrade," Nuclear Fusion **52** (2012), 10.1088/0029-5515/52/8/083013.

[6]E. Viezzer, T. Pütterich, E. Fable, A. Bergmann, R. Dux, R. M. McDermott, R. M. Churchill, and M. G. Dunne, "Rotation and density asymmetries in the presence of large poloidal impurity flows in the edge pedestal," Plasma Physics and Controlled Fusion **55** (2013), 10.1088/0741-3335/55/12/124037.

[7]R. M. Churchill, B. Lipschultz, and C. Theiler, "In-out impurity density asymmetry in the pedestal region of alcator c-mod," Nuclear Fusion **53** (2013), 10.1088/0029-5515/53/12/122002.

[8]R. M. Churchill, C. Theiler, B. Lipschultz, I. H. Hutchinson, M. L. Reinke, D. Whyte, J. W. Hughes, P. Catto, M. Landreman, D. Ernst, C. S. Chang, R. Hager, A. Hubbard, P. Ennever, and J. R. Walk, "Poloidal asymmetries in edge transport barriers," Physics of Plasmas **22** (2015), 10.1063/1.4918353.

[9]D. J. Cruz-Zabala, E. Viezzer, M. Griener, U. Plank, M. Cavedon, P. Cano-Megias, R. Dux, G. Fuchert, J. Garcia-Lopez, M. Garcia-Munoz, A. J. van Vuuren, T. Pütterich, and V. Rohde, "Upgrade of the edge charge exchange recombination spectroscopy system at the high field side of asdex upgrade," Journal of Instrumentation **14**, C11006 (2019).

[10]D. J. Cruz-Zabala, E. Viezzer, P. Cano-Megias, M. Cavedon, R. Dux, U. Plank, T. Pütterich, K. McKay, A. Rodriguez-Gonzalez, and M. Garcia-Munoz, "Poloidal structure of the edge parallel flow in h-mode, l-mode and i-mode confinement regimes," Nuclear Fusion **64**, 076051 (2024).

[11]H. Zohm, "Edge localized modes (elms)," Plasma Physics and Controlled Fusion **38**, 105 (1996).

[12]A. W. Leonard, "Edge-localized-modes in tokamaks," Physics of Plasmas **21** (2014), 10.1063/1.4894742.

[13]A. Mancini, J. Ayllon-Guerola, S. J. Doyle, M. Agredano-Torres, D. Lopez-Aires, J. Toledo-Garrido, E. Viezzer, M. Garcia-Muñoz, P. F. Buxton, K. J. Chung, J. Garcia-Dominguez, J. Garcia-Lopez, M. P. Gryaznevich, J. Hidalgo-Salaverri, Y. S. Hwang, and J. Segado-Fernández, "Mechanical and electromagnetic design of the vacuum vessel of the smart tokamak," Fusion Engineering and Design **171**, 112542 (2021).

[14]M. Agredano-Torres, J. L. Garcia-Sanchez, A. Mancini, S. J. Doyle, M. Garcia-Munoz, J. Ayllon-Guerola, M. Barragan-Villarejo, E. Viezzer, J. Segado-Fernandez, D. Lopez-Aires, J. Toledo-Garrido, P. F. Buxton, K. J. Chung, J. Garcia-Dominguez, L. Garcia-Franquelo, M. P. Gryaznevich, J. Hidalgo-Salaverri, Y. S. Hwang, J. I. Leon-Galvan, and J. Maza-Ortega, "Coils and power supplies design for the smart tokamak," Fusion Engineering and Design **168**, 112683 (2021).

[15]S. J. Doyle, D. Lopez-Aires, A. Mancini, M. Agredano-Torres, J. L. Garcia-Sanchez, J. Segado-Fernandez, J. Ayllon-Guerola, M. Garcia-Muñoz, E. Viezzer, C. Soria-Hoyo, J. Garcia-Lopez, G. Cunningham, P. F. Buxton, M. P. Gryaznevich, Y. S. Hwang, and K. J. Chung, "Magnetic equilibrium design for the smart tokamak," Fusion Engineering and Design **171**, 112706 (2021).

[16]J. E. Menard, S. C. Jardin, S. M. Kaye, C. E. Kessel, and J. Manickam, "Ideal mhd stability limits of low aspect ratio tokamak plasmas," Nuclear Fusion **37**, 595 (1997).

[17]Y. K. Peng, "The physics of spherical torus plasmas," Physics of Plasmas **7**, 1681–1692 (2000).

[18]J. E. Menard, T. Brown, L. El-Guebaly, M. Boyer, J. Canik, B. Colling, R. Raman, Z. Wang, Y. Zhai, P. Buxton, B. Covele, C. D'Angelo, A. Davis, S. Gerhardt, M. Gryaznevich, M. Harb, T. C. Hender, S. Kaye, D. Kingham, M. Kotschenreuther, S. Mahajan, R. Maingi, E. Marriott, E. T. Meier, L. Mynsberge, C. Neumeyer, M. Ono, J. K. Park, S. A. Sabbagh, V. Soukhanovskii, P. Valanju, and R. Woolley, "Fusion nuclear science facilities and pilot plants based on the spherical tokamak," Nuclear Fusion **56**, 106023 (2016).

[19]W. W. Heidbrink, D. Liu, Y. Luo, E. Ruskov, and B. Geiger, "A code that simulates fast-ion d_α and neutral particle measurements," Communications in Computational Physics **10**, 716–741 (2011).

[20]B. Geiger, L. Stagner, W. W. Heidbrink, R. Dux, R. Fischer, Y. Fujiwara, A. V. Garcia, A. S. Jacobsen, A. J. V. Vuuren, A. N. Karpushov, D. Liu, P. A. Schneider, I. Sfiligoi, P. Z. Poloskei, and M. Weiland, "Progress in modelling fast-ion d-alpha spectra and neutral particle analyzer fluxes using fidasim," Plasma Physics and Controlled Fusion **62** (2020), 10.1088/1361-6587/aba8d7.

[21]M. Griener, O. Schmitz, K. Bald, D. Bösser, M. Cavedon, P. D. Marné, T. Eich, G. Fuchert, A. Herrmann, A. Kappatou, T. Lunt, V. Rohde, B. Schweer, M. Sochor, U. Stroth, A. Terra, and E. Wolfrum, "Fast piezoelectric valve offering controlled gas injection in magnetically confined fusion plasmas for diagnostic and fuelling purposes," Review of Scientific Instruments **88** (2017), 10.1063/1.4978629.